

Effect of quantum measurement errors on witnessing network topology

Shu-Yuan Yang(杨舒媛), Kan He(贺衍), and Ming-Xing Luo(罗明星)
Citation: Chin. Phys. B, 2025, 34 (**9**): 090302. DOI: 10.1088/1674-1056/ade3af
http://cpb.iphy.ac.cn; http://iopscience.iop.org/cpb

What follows is a list of articles you may be interested in

Witnessing the distribution of sources in quantum networks via hierarchical nonlocality

Shu-Yuan Yang(杨舒媛), Jin-Chuan Hou(侯晋川), and Kan He(贺衍)
Chin. Phys. B, 2025, 34 (**6**): 060303. DOI: 10.1088/1674-1056/add507

Measurement-based entanglement purification for hybrid entangled state

Cheng-Chen Luo(罗程晨), Shi-Pu Gu(顾世浦), Xing-Fu Wang(王兴福), Lan Zhou(周澜), and Yu-Bo Sheng(盛宇波)
Chin. Phys. B, 2025, 34 (**3**): 030307. DOI: 10.1088/1674-1056/adb267

Multi-protocol relay chaining for large-scale quantum key distribution networks

Yuan Cao(曹原), Xiaosong Yu(郁小松), Yongli Zhao(赵永利), Chunhui Zhang(张春辉), Xingyu Zhou(周星宇), Jie Zhang(张杰), and Qin Wang(王琴)
Chin. Phys. B, 2025, 34 (**1**): 010310. DOI: 10.1088/1674-1056/ad9018

Multi-hop quantum teleportation based on HSES via GHZ-like states

She-Xiang Jiang(蒋社想), Xiao-Long Wei(韦晓龙), Jin-Huan Li(李金欢), and Shuai-Shuai Li(李帅帅)
Chin. Phys. B, 2025, 34 (**1**): 010302. DOI: 10.1088/1674-1056/ad8db0

Security analysis of satellite-to-ground reference-frame-independent quantum key distribution with beam wandering

Chun Zhou(周淳), Yan-Mei Zhao(赵燕美), Xiao-Liang Yang(杨晓亮), Yi-Fei Lu(陆宜飞), Yu Zhou(周雨), Xiao-Lei Jiang(姜晓磊), Hai-Tao Wang(汪海涛), Yang Wang(汪洋), Jia-Ji Li(李家骥), Mu-Sheng Jiang(江木生), Xiang Wang(汪翔), Hai-Long Zhang(张海龙), Hong-Wei Li(李宏伟), and Wan-Su Bao(鲍皖苏)
Chin. Phys. B, 2024, 33 (**8**): 080306. DOI: 10.1088/1674-1056/ad51f6

SPECIAL TOPIC — Quantum communication and quantum network

Effect of quantum measurement errors on witnessing network topology

Shu-Yuan Yang(杨舒媛)[1], Kan He(贺衍)[2,†], and Ming-Xing Luo(罗明星)[3,‡]

[1] *School of Mathematics, North University of China, Taiyuan* 030051, *China*
[2] *College of Mathematics, Taiyuan University of Technology, Taiyuan* 030024, *China*
[3] *School of Information Science and Technology, Southwest Jiaotong University, Chengdu* 610031, *China*

(Received 15 May 2025; revised manuscript received 10 June 2025; accepted manuscript online 12 June 2025)

The fragility and stochastic behavior of quantum sources make it crucial to witness the topology of quantum networks. Most previous theoretical methods are based on perfect assumptions of quantum measurements. In this work, we propose a method to witness network topology under imperfect assumptions of quantum measurements. We show that the discrimination between star and triangle networks depends on the specific error tolerances of local measurements. This extends recent results for witnessing the triangle network [*Phys. Rev. Lett.* **132** 240801 (2024)].

Keywords: quantum network, quantum measurement, error

PACS: 03.67.–a, 03.67.Hk

DOI: 10.1088/1674-1056/ade3af **CSTR:** 32038.14.CPB.ade3af

1. Introduction

Quantum networks are rapidly advancing, promising significant benefits in computing, sensing, and secure communications.[1–10] As the backbone of quantum communication and distributed quantum computing, quantum networks enable the distribution of entanglement and quantum information across distant nodes.[11] However, the practical deployment of quantum networks faces significant challenges, stemming from their inherent fragility and stochastic operational characteristics during their generation, transmission, and storage.[12–14] These limitations underscore the critical importance of understanding and optimizing the topology of quantum networks, which directly affects the efficiency of information transfer[15] and the feasibility of implementing advanced quantum protocols.[16]

So far, several methods have been proposed for distinguishing network topologies. The first method is based on the von Neumann entropy and mutual information[17,18] to distinguish network topologies. These studies are limited to distinguishing quantum networks that utilize specific source states, such as particular pure states or noisy states. Another method uses the concept of fidelity for distinguishing the topological structures of six-qubit photonic networks.[19] As a quantum correlation, Bell nonlocality, when combined with quantum networks, offers fresh viewpoints for understanding network topology. These include nonlocality in different network structures,[20–24] genuine network nonlocality,[25] full network nonlocality (FNN),[26,27] and hierarchical network nonlocality.[28,29] Subsequently, some new techniques for witnessing network topologies have been developed[30,31] by using nonlocal correlations. Interestingly, Mao *et al.*[30] introduced a Bell-type witness operator, as shown in Fig. 1. This method can not only certify the network topology but also witness the network nonlocal correlation by different levels of violations. This inspires us to distinguish general networks with quantum correlations.

Notably, quantum measurement emerges as the essential tool for distinguishing network topologies through the lens of nonlocality, given that the detection of network nonlocality hinges on quantum measurement. However, practical measurements are inevitably subject to imperfections.[32–34] These imperfections may obscure the signatures of network nonlocality, rendering existing measurement schemes for witnessing network topologies unreliable in real-world scenarios.

In this paper, we develop a method for witnessing network topologies under imperfect measurement assumptions. Recall that Morelli *et al.*[35] established a foundational framework for quantifying imperfect measurements, which has been applied to analyzing the detection of genuine multipartite entanglement[36] and quantum steering.[37] Building on these insights into imperfect measurements, we focus on the robustness of topology discrimination in star and triangle quantum networks.

†Corresponding author. E-mail: hekan@tyut.edu.cn; hekanquantum@163.com
‡Corresponding author. E-mail: mxluo@swjtu.edu.cn

© 2025 Chinese Physical Society and IOP Publishing Ltd. All rights, including for text and data mining, AI training, and similar technologies, are reserved.

2. Preliminary

2.1. Witnessing triangle network topologies

To distinguish the five network topologies illustrated in Fig. 1, Ref. [30] proposed the measurement scheme denoted by $\mathcal{B}$:

$$\begin{aligned}\langle\mathcal{B}\rangle :=& \\ \alpha[&\langle A_0B_0(C_0+C_1)\rangle+\langle A_1B_1(C_0-C_1)\rangle+\langle A_2(B_2+B_3)C_2\rangle \\ &+\langle A_2(B_2-B_3)C_2\rangle+\langle(A_4+A_5)B_4C_4\rangle+\langle(A_4-A_5)B_4C_4\rangle] \\ &+\langle A_0(C_0+C_1)\rangle+\langle A_0(C_0-C_1)\rangle+\langle(B_2+B_3)C_2\rangle \\ &+\langle(B_2-B_3)C_2\rangle+\langle(A_4+A_5)B_4\rangle+\langle(A_4-A_5)B_4\rangle, \end{aligned} \tag{1}$$

where A_i, B_j, and C_k are observables performed by parties A, B, and C, respectively, and $\alpha \geq 0$. For each network N_m described in Fig. 1, we denote $S_{N_m} = \max_{A_i,B_j,C_k}\langle\mathcal{B}\rangle$ with $m = 0,1,1',2$, and 3. Mao *et al.*[30] showed that $S_{N_0} < S_{N_1} < S_{N_{1'}} < S_{N_2} < S_{N_3}$ when $\alpha = 2$. This can be utilized to distinguish the five networks.

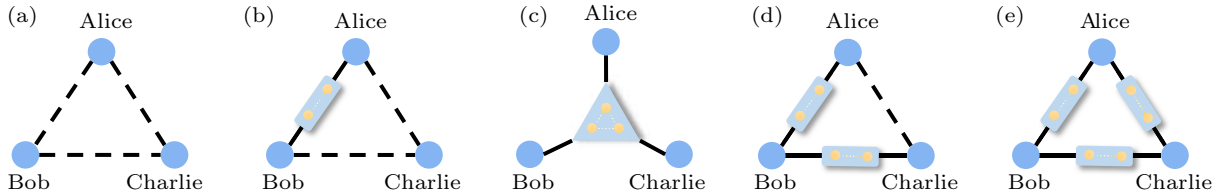


Fig. 1. Triangle quantum networks involving three parties, Alice, Bob, and Charlie, can exhibit five distinct network topologies. (a) N_0: the three parties are only connected through classical variables (indicated by dashed lines). The remaining configurations, shown in panels (b)–(e), involve different combinations of quantum and classical sources. (b) N_1: one bipartite entangled source and two classical variables. (c) $N_{1'}$: a tripartite entangled source. (d) N_2: two bipartite entangled sources and one classical variable. (e) N_3: three bipartite entangled sources. All these configurations maintain cyclic symmetry. Here, the entangled pairs are denoted by the yellow label $(\circ\cdots\circ)$.

2.2. Imperfection in measurement

We review the quantification of imprecise measurements and the concept of detection efficiency. In Ref. [35], the error in the measurements is quantified by comparing the target measurement set $\{M_{a|x}\}$ with the associated lab measurement set $\{\tilde{M}_{a|x}\}$ using the average fidelity

$$\mathcal{F}_x \equiv \frac{1}{d}\sum_{a=1}^{o}\mathrm{tr}(M_{a|x}\tilde{M}_{a|x}), \tag{2}$$

where d represents the local dimension of the bipartite state being measured, and the subsystems are measured with input x, producing output $a \in \{1,2,\ldots,o\}$. The average fidelity $\mathcal{F}_x \in [0,1]$, with $\mathcal{F}_x = 1$ if and only if the lab measurement perfectly matches the target measurement.

Another kind of imperfect measurements is defined by detection efficiency. The measurement device may fail to work with a certain probability $1-\eta$. Ideally, the output probability after the measurement operator $M_{a|x}$ acts on the quantum state ρ_A is $p(a|x) = \mathrm{tr}(M_{a|x}\rho_A)$. However, if the efficiency of each detector is η, the actual output probability becomes $p'(a|x) = \eta\,\mathrm{tr}(M_{a|x}\rho_A) = \eta\,p(a|x)$.

2.3. Violating Clauser–Horne–Shimony–Holt (CHSH) inequality with imperfect measurements

In the bipartite Bell scenario, suppose that Alice and Bob share a bipartite state ρ_{AB} and perform binary input and output measurements. Let A_0, A_1 and B_0, B_1 be the observables for Alice and Bob, respectively, corresponding to binary inputs $0,1$. It is proved that, in this case, the local correlation necessarily satisfies the CHSH inequality,[38,39] i.e.,

$$\langle A_0(B_0+B_1)\rangle + \langle A_1(B_0-B_1)\rangle \leq 2. \tag{3}$$

If Alice and Bob share a 2-qubit maximally entangled state, then the maximum quantum violation of $2\sqrt{2}$ can be reached. Here, the ideal measurement schemes are considered as follows:

$$A_0 = \sigma_z,\ \ A_1 = \sigma_x, \tag{4}$$

$$B_0 = \frac{1}{\sqrt{2}}(\sigma_z+\sigma_x),\ \ B_1 = \frac{1}{\sqrt{2}}(\sigma_z-\sigma_x), \tag{5}$$

where σ_z and σ_x are Pauli matrices. These measurements are called target measurements. The measurement operators corresponding to A_x and B_y are represented as $\{A_{a|x}\}$ and $\{B_{b|y}\}$, respectively. However, the measurements actually performed in the lab do not precisely correspond to the target measurements, but instead to positive operator valued measures (POVMs) $\{\tilde{A}_{a|x}\}$ and $\{\tilde{B}_{b|y}\}$. We quantify the correspondence between each of the target measurements and the associated lab measurements through their average fidelity,

$$\mathcal{F}_x^A \equiv \frac{1}{2}\left(\mathrm{tr}(A_{0|x}\tilde{A}_{0|x}) + \mathrm{tr}(A_{1|x}\tilde{A}_{1|x})\right), \tag{6}$$

$$\mathcal{F}_y^B \equiv \frac{1}{2}\left(\mathrm{tr}(B_{0|y}\tilde{B}_{0|y}) + \mathrm{tr}(B_{1|y}\tilde{B}_{1|y})\right). \tag{7}$$

The fidelities $\{\mathcal{F}_x^A, \mathcal{F}_y^B\}$ can be directly determined by probing the lab measurements with single qudits from a well-calibrated auxiliary source. Assuming that each measurement device is not perfectly controlled, there is a lower bound on fidelity, that is,

$$\mathcal{F}_x^A \geq 1-\varepsilon_x^A,\ \ \mathcal{F}_y^B \geq 1-\varepsilon_y^B. \tag{8}$$

Here, the parameter $\varepsilon \in [0,1]$ represents the inaccuracy of the lab measurement.

If we allow the lab observables to have an ε-deviation with respect to the target measurements $\{A_0, A_1, B_0, B_1\}$, then this corresponds to the following constraints:

$$\mathrm{tr}(A_x\tilde{A}_x) \geq 2-4\varepsilon, \quad \mathrm{tr}(B_y\tilde{B}_y) \geq 2-4\varepsilon. \tag{9}$$

Since the measurement operators are fully characterized by their corresponding Bloch vectors, we can, without loss of generality, restrict our analysis to the XZ-plane of the Bloch sphere. We write

$$\tilde{A}_0 = \cos\theta_1\sigma_x + \sin\theta_1\sigma_z, \tag{10}$$

$$\tilde{A}_1 = \cos\theta_2\sigma_x + \sin\theta_2\sigma_z, \tag{11}$$

$$\tilde{B}_0 = \cos\theta_3\sigma_x + \sin\theta_3\sigma_z, \tag{12}$$

$$\tilde{B}_1 = \cos\theta_4\sigma_x - \sin\theta_4\sigma_z. \tag{13}$$

Thus, in the relevant case of equality, the fidelity condition described by Eq. (9) becomes

$$\theta_1 = \arcsin(1-2\varepsilon), \tag{14}$$

$$\theta_2 = \arccos(1-2\varepsilon), \tag{15}$$

$$\theta_3 = \theta_4 = \arcsin(1-2\varepsilon) - \pi/4. \tag{16}$$

Based on the above analysis, when performing imprecise measurements with inaccuracy ε in the lab, the maximum value of the CHSH inequality is achieved as $2\sqrt{2}(1-2\varepsilon)^2$. This result is obtained under the measurement scheme and parameter constraints given in Eqs. (10)–(16).

3. Witnessing star network topology

We first focus on the star network composed of four parties and three sources, as illustrated in Fig. 2. The largest difference among the four network structures is the amount of quantum sources. Therefore, we first propose a method to distinguish the four network topologies based on their respective numbers of quantum sources. For this, we propose a network correlation measurement, denoted as $\mathcal{Q}$, and define

$$\begin{aligned}\langle\mathcal{Q}\rangle \;=\; & |\langle A^+D_0B_1^+\rangle|^{1/2} + |\langle A^-D_1B_1^-\rangle|^{1/2} \\ & + |\langle A^+D_2C_1^+\rangle|^{1/2} + |\langle A^-D_3C_1^-\rangle|^{1/2} \\ & + |\langle B_2^+D_4C_2^+\rangle|^{1/2} + |\langle B_2^-D_5C_2^-\rangle|^{1/2}.\end{aligned} \tag{17}$$

Here, $A^\pm = A_0 \pm A_1$, $B_i^\pm = B_{i0} \pm B_{i1}$, and $C_j^\pm = C_{j0} \pm C_{j1}$, where A_0, A_1, B_{i0}, B_{i1}, C_{j0}, C_{j1}, and D_s represent the observables performed by parties A, B, C, and D, respectively ($i, j \in \{1,2\}, s \in \{0,1,\ldots,5\}$). The expectation values are given by $\langle A_xD_{s_1}B_{1y}\rangle = \sum_{a,b,d=-1,1} abdP(a,d,b|x,s_1,y)$, $\langle A_xD_{s_2}C_{1z}\rangle = \sum_{a,c,d=-1,1} acdP(a,d,c|x,s_2,z)$, and $\langle B_{2y}D_{s_3}C_{2z}\rangle = \sum_{b,c,d=-1,1} bcdP(b,d,c|y,s_3,z)$. Here, x, y, z, and s_i represent the inputs of the measurement, while a, b, c, and d represent the corresponding outputs.

Without loss of generality, we consider four distinct network topologies corresponding to the number of quantum sources in the network being 0, 1, 2, and 3, respectively. These are represented by the network topologies M_0, M_1, M_2, and M_3 as shown in Fig. 2. Let us consider the quantum states $|\Phi^+\rangle_{AD}$, $|\Phi^+\rangle_{AD}\otimes|\Phi^+\rangle_{BD'}$, and $|\Phi^+\rangle_{AD}\otimes|\Phi^+\rangle_{BD'}\otimes|\Phi^+\rangle_{CD''}$ respectively for network topology M_1, M_2, and M_3, where $|\Phi^+\rangle_{XD} = (|00\rangle_{XD} + |11\rangle_{XD})/\sqrt{2}$ ($X \in \{A,B,C\}$). For each topology shown in Fig. 2, we can always optimize its measurement scheme and thus obtain the upper bound of $\langle\mathcal{Q}\rangle$ corresponding to different network structures. Specifically,

$$\langle\mathcal{Q}\rangle \leq S_{M_n}, \tag{18}$$

where $S_{M_n} \equiv \max_{A_x,B_{jy},C_{kz},D_s}\langle\mathcal{Q}\rangle$, with $n = 0,1,2,3$ denoting the different network topologies. Intriguingly, we note that each optimal measurement scheme consists of independent local measurements.

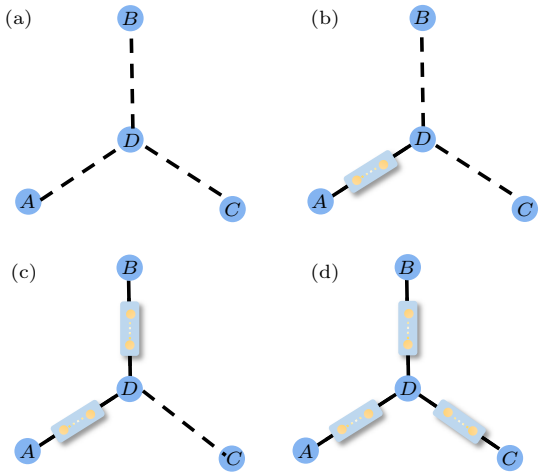


Fig. 2. Star quantum networks involving four parties (A, B, C, and D) can exhibit four distinct network topologies. In (a) M_0, the four parties are only connected through classical variables (indicated by dashed lines). In (b) M_1, (c) M_2, and (d) M_3, there are 1, 2, and 3 entangled pairs distributed, respectively. Here, the entangled pairs are denoted by $(\circ\cdots\circ)$.

For the network M_0 shown in Fig. 2(a), all the sources are classical variables. Since all subnetworks in the star network adhere to the local hidden variable model, the upper bound of the inequality is always 6, that is,

$$S_{M_0} = 6.$$

For any $n \in \{1,2,3\}$, we can always obtain the value of S_{M_n} by optimizing the measurements A_x, B_{iy}, C_{jz}, and D_s independently for each network topology. For example, for the quantum network shown in Fig. 2(b), we get $S_{M_1} = 2+2^{9/4}$ with the following set of measurements,

$$A_0 = \frac{1}{\sqrt{2}}(\sigma_z+\sigma_x), \quad A_1 = \frac{1}{\sqrt{2}}(\sigma_z-\sigma_x), \tag{19}$$

$$D_0 = D_2 = \sigma_z, \quad D_1 = D_3 = \sigma_x, \quad D_4 = D_5 = I_2, \tag{20}$$

where $\sigma_{x,z}$ are Pauli matrices and I_2 is the identity operation. The choice of measurement scheme depends on the position of

the quantum state. Meanwhile, as parties B and C only receive classical variables, measurements can always be chosen such that

$$\langle B_{10}\rangle = \langle B_{20}\rangle = 1,\ \langle B_{11}\rangle = \langle B_{21}\rangle = 0, \tag{21}$$

$$\langle C_{10}\rangle = \langle C_{20}\rangle = 1,\ \langle C_{11}\rangle = \langle C_{21}\rangle = 0 \tag{22}$$

hold.

For further details of the proof and the measurement schemes corresponding to Figs. 2(b)–2(d), please refer to Appendix A. Under these schemes, we can always calculate the value of S_{M_n} for the network topology M_n, with the upper bounds listed in Table 1. Note that for each topology, we assume a specific distribution of quantum sources. In practice, if the positions of the quantum sources change, we simply need to adjust our measurement schemes accordingly. Interestingly, we find that even when the positions of the quantum sources are altered, the value of S_{M_n} remains unchanged for any $n \in \{0,1,2,3\}$.

Table 1. The upper bounds of Eq. (17) for different star network topologies.

Network topology	Upper bound S_{M_n}
M_0	$S_{M_0} = 6$
M_1	$S_{M_1} = 2+2^{9/4}$
M_2	$S_{M_2} = 2\sqrt{2}+2^{9/4}$
M_3	$S_{M_3} = 6\sqrt{2}$

Next, we show below that exceeding the upper bounds listed in Table 1 can certify the number of quantum sources in the network. First, each party attempts to use the optimal measurements under various scenarios, and we can calculate the value of $\langle\mathcal{Q}\rangle$. This value indicates the number of quantum sources in the network. Specifically, if the value of $\langle\mathcal{Q}\rangle$ exceeds S_{M_0}, it indicates that there must be at least one quantum source in the network, which may correspond to the topologies M_1, M_2, and M_3. In addition, if the value of $\langle\mathcal{Q}\rangle$ belongs to $[S_{M_0}, S_{M_1}]$, then there is one quantum source in the network. If the value of $\langle\mathcal{Q}\rangle$ exceeds S_{M_1} and is simultaneously less than S_{M_2}, there are two quantum sources. If the value of $\langle\mathcal{Q}\rangle$ exceeds S_{M_2}, all sources in the network are quantum sources. Thus, we can distinguish the four networks in Fig. 2.

It is also mentioned that the aforementioned method can be extended to distinguish the topology of star networks with arbitrary numbers of parties. To achieve this, we decompose each network into entanglement swapping subnetworks and analyze them accordingly. Moreover, one can utilize CHSH inequalities to determine the location of each quantum source within the four star networks depicted in Fig. 2.

4. Quantum network topology discrimination with imperfect measurements

Here we study the impact of measurement imperfections on network topology discrimination on two network structures: star and triangle networks.

4.1. Star networks

Let us first introduce the imperfect measurements performed by the parties involved in the quantity $\langle\mathcal{Q}\rangle$. In the ideal case, the two local observables on party D may include σ_z and σ_x. Assume that the forms of the imprecise measurements of σ_z and σ_x are

$$\tilde{\sigma}_z = \cos\theta_1\sigma_x + \sin\theta_1\sigma_z, \tag{23}$$

$$\tilde{\sigma}_x = \cos\theta_2\sigma_x + \sin\theta_2\sigma_z. \tag{24}$$

Due to the limitations introduced by measurement errors, we require $\theta_1 = \arcsin(1-2\varepsilon)$ and $\theta_2 = \arccos(1-2\varepsilon)$. For the remaining parties, the measurements performed are only in two cases, $w_1 = (\sigma_z+\sigma_x)/\sqrt{2}$ and $w_2 = (\sigma_z-\sigma_x)/\sqrt{2}$. Therefore, we still consider their imprecise measurement forms to be

$$\tilde{w}_1 = \cos\theta_3\sigma_x + \sin\theta_3\sigma_z, \tag{25}$$

$$\tilde{w}_2 = \cos\theta_4\sigma_x - \sin\theta_4\sigma_z. \tag{26}$$

Similarly, under the influence of the measurement imprecision ε, we determine $\cos\theta_3 + \sin\theta_3 = \sqrt{2}(1-2\varepsilon)$ and $\theta_3 = \theta_4$.

To illustrate the impact of error ε on network topology discrimination, we calculate the values of S_{M_n} for different network structures under the influence of measurement error ε for any $n \in \{0,1,2,3\}$. These values are listed in Table 2 for the network topology M_n. The detailed proof is provided in Appendix B.

Table 2. The upper bound of Eq. (17) under different star network topologies with the influence of imprecise measurement. Here $H(\varepsilon) = 2^{7/4}[(1-2\varepsilon)^2 + (1-2\varepsilon)(1-8\varepsilon+8\varepsilon^2)^{1/2}]^{1/2}$.

Network topology	Upper bound S_{M_n}
M_0	$S_{M_0} = 6$
M_1	$S_{M_1} = 2+H(\varepsilon)$
M_2	$S_{M_2} = 2\sqrt{2}(1-2\varepsilon)^2 + H(\varepsilon)$
M_3	$S_{M_3} = 6\sqrt{2}(1-2\varepsilon)^2$

Next, we calculate the differences $S_{M_{i+1}} - S_{M_i}$ for $i \in \{0,1,2\}$, and present these values in Fig. 3. This analysis indicates that as long as the measurement error is controlled within $\varepsilon \in [0, 0.0613]$, the method proposed in Section 3 remains effective for determining the number of quantum sources in the star network depicted in Fig. 2. Subsequently, the CHSH inequality can be used to identify the positions of these quantum sources.

In order to account for the impact of detection efficiency on this method, we still need to compute S_{M_i} across different scenarios. We use S'_{M_i} to denote the upper bound when influenced by detection efficiency η. The specific values are listed in Table 3. Based on the results in Fig. 4, it can be inferred

that the method for witnessing network topology proposed in Section 3 remains effective when $\eta > 0.8409$. This is because, under these conditions, the inequality $S'_{M_0} < S'_{M_1} < S'_{M_2} < S'_{M_3}$ can always hold.

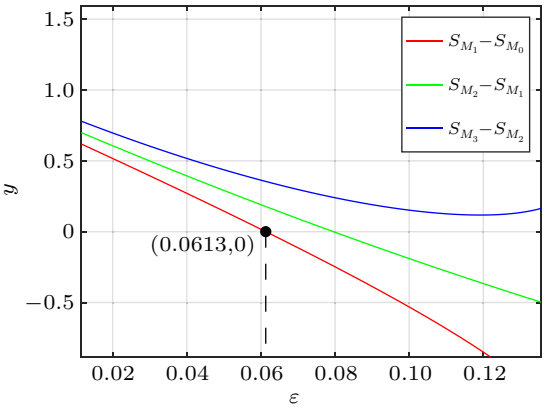


Fig. 3. The x-axis represents the measurement imprecision ε. The red, green, and blue curves correspond to the values of $S_{M_1}-S_{M_0}$, $S_{M_2}-S_{M_1}$, and $S_{M_3}-S_{M_2}$ as functions of the imprecision ε, respectively.

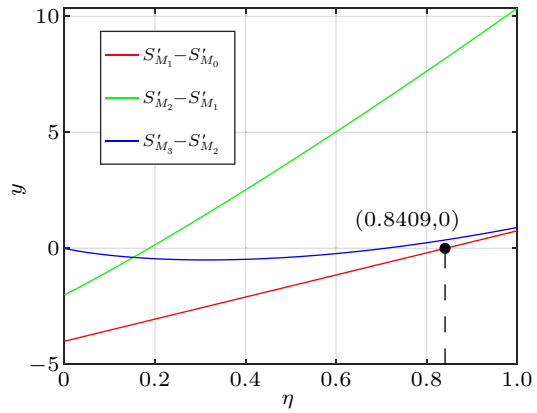


Fig. 4. The x-axis represents the detection efficiency η. The red, green, and blue curves correspond to the values of $S'_{M_1}-S'_{M_0}$, $S'_{M_2}-S'_{M_1}$, and $S'_{M_3}-S'_{M_2}$ as the function of the detection efficiency η, respectively.

Table 3. For different realizations of the star network, this table shows the upper bound of S'_{M_n} under the influence of detection efficiency η.

Network topology	Upper bound S'_{M_n}
M_0	$S'_{M_0}=6$
M_1	$S'_{M_1}=2+2^{9/4}\eta$
M_2	$S'_{M_2}=2\sqrt{2}\eta^{3/2}+2^{9/4}\eta$
M_3	$S'_{M_3}=6\sqrt{2}\eta^{3/2}$

4.2. Triangle networks

For the triangle network depicted in Fig. 1, we compute the upper bounds of the Bell-type witness operators $\mathcal{B}$ for different network topologies under imperfect measurements. Similarly, when the local measurements performed by the parties involve σ_z, σ_x, $w_1=(\sigma_z+\sigma_x)/\sqrt{2}$, and $w_2=(\sigma_z-\sigma_x)/\sqrt{2}$, these measurements are modified to

$$\tilde{\sigma}_z = \cos\theta_1\sigma_x + \sin\theta_1\sigma_z, \tag{27}$$

$$\tilde{\sigma}_x = \cos\theta_2\sigma_x + \sin\theta_2\sigma_z, \tag{28}$$

$$\tilde{w}_1 = \cos\theta_3\sigma_x + \sin\theta_3\sigma_z, \tag{29}$$

$$\tilde{w}_2 = \cos\theta_4\sigma_x - \sin\theta_4\sigma_z, \tag{30}$$

where $\theta_1=\arcsin(1-2\varepsilon)$, $\theta_2=\arccos(1-2\varepsilon)$, $\cos\theta_3+\sin\theta_3=\sqrt{2}(1-2\varepsilon)$, and $\theta_3=\theta_4$. In the subsequent analysis, whenever we consider the imprecise measurements in the experimental process, we adopt the measurement scheme shown in Eqs. (27)–(30).

Next, for convenience, we provide an example of the network topology N_1, where Alice and Bob share an Einstein–Podolsky–Rosen (EPR) state $|\Phi^+\rangle_{AB}=(|00\rangle_{AB}+|11\rangle_{AB})/\sqrt{2}$. In the ideal case, the result in Ref. [30] shows that we attain S_{N_1} when

$$\langle A_0\rangle=\langle B_0\rangle=\langle C_0\rangle=\langle A_1\rangle=\langle B_1\rangle=\langle C_1\rangle=1, \tag{31}$$

classical :

$$\langle A_2\rangle=\langle B_2\rangle=\langle C_2\rangle=\langle A_3\rangle=\langle B_3\rangle=\langle C_3\rangle=1, \tag{32}$$

quantum :

$$B_2=\frac{1}{\sqrt{2}}(\sigma_z+\sigma_x),\ \ B_3=\frac{1}{\sqrt{2}}(\sigma_z-\sigma_x), \tag{33}$$

$$A_2=\sigma_z,\ \ A_3=\sigma_x,\ \ \langle C_2\rangle=\langle C_3\rangle=1, \tag{34}$$

$$A_4=\frac{1}{\sqrt{2}}(\sigma_z+\sigma_x),\ \ A_5=\frac{1}{\sqrt{2}}(\sigma_z-\sigma_x), \tag{35}$$

$$B_4=\sigma_z,\ \ B_5=\sigma_x,\ \ \langle C_4\rangle=\langle C_5\rangle=1. \tag{36}$$

However, each party performs imprecise measurements with inaccuracy ε. At this point, the measurement schemes for parties A and B, who share the quantum state $|\Phi^+\rangle_{AB}=(|00\rangle_{AB}+|11\rangle_{AB})/\sqrt{2}$, are modified to

$$\tilde{A}_2=\tilde{B}_4=\cos\theta_1\sigma_x+\sin\theta_1\sigma_z, \tag{37}$$

$$\tilde{A}_3=\tilde{B}_5=\cos\theta_2\sigma_x+\sin\theta_2\sigma_z, \tag{38}$$

$$\tilde{B}_2=\tilde{A}_4=\cos\theta_3\sigma_x+\sin\theta_3\sigma_z, \tag{39}$$

$$\tilde{B}_3=\tilde{A}_5=\cos\theta_4\sigma_x-\sin\theta_4\sigma_z, \tag{40}$$

where $\theta_1=\arcsin(1-2\varepsilon)$, $\theta_2=\arccos(1-2\varepsilon)$, $\cos\theta_3+\sin\theta_3=\sqrt{2}(1-2\varepsilon)$, and $\theta_3=\theta_4$. In this case, we get a new upper bound as

$$S_{N_1}=\begin{cases}(\alpha+1)[2\sqrt{2}(1-2\varepsilon)^2+4], & \text{if } \alpha\le f_1(\varepsilon),\\ (2\alpha+1)[2\sqrt{2}(1-2\varepsilon)^2+1]+1, & \text{if } \alpha>f_1(\varepsilon),\end{cases}$$

where $f_1(\varepsilon)=1/[\sqrt{2}(1-2\varepsilon)^2-1]$. The details of the calculation are provided in Appendix C. In other cases, the upper bound of $\langle\mathcal{B}\rangle$ can also be calculated using a similar method.

Based on the previous discussion, we derive upper bounds for Bell-type witness operators $\mathcal{B}$ and list them in Table 4. For the network topology in Fig. 1, where each source is classical, the upper bound is always $6(1+\alpha)$. Besides, these upper bounds depend on two key factors: the measurement inaccuracy ε and the parameter α in $\mathcal{B}$. To assess the robustness of

this approach, for different inaccuracies ε, we search for the value of the parameter α. If the values of $\langle\mathcal{B}\rangle$ differ among the five network structures, then the network topology can still be distinguished.

Table 4. Upper bounds of S_{N_n} in different realizations of the triangle network, considering the influence of imprecise measurement. Here $\theta_5=\theta-\arccos(1-2\varepsilon)$, $\theta=\arcsin((\alpha+1)/(2\alpha^2+2\alpha+1)^{1/2})$, $f_1(\varepsilon)=1/[\sqrt{2}(1-2\varepsilon)^2-1]$, and $F(\varepsilon)=2\sqrt{2}(1-2\varepsilon)^2$.

Network topology	Upper bound S_{N_m}
N_0	$S_{N_0}=6\alpha+6$
N_1	$S_{N_1}=\begin{cases}(\alpha+1)\big(F(\varepsilon)+4\big), & \text{if } \alpha\le f_1(\varepsilon),\\ (2\alpha+1)\big(F(\varepsilon)+1\big)+1, & \text{if } \alpha>f_1(\varepsilon)\end{cases}$
$N_{1'}$	$S_{N_{1'}}=6[(\alpha+1)(1-2\varepsilon)\cos\theta_5+2\alpha(1-2\varepsilon)^2\sin\theta_5]$
N_2	$S_{N_2}=\begin{cases}2\alpha+2+2F(\varepsilon)(\alpha+1), & \text{if } \alpha\le f_1(\varepsilon),\\ F(\varepsilon)(3\alpha+2), & \text{if } \alpha>f_1(\varepsilon)\end{cases}$
N_3	$S_{N_3}=3F(\varepsilon)(\alpha+1)$

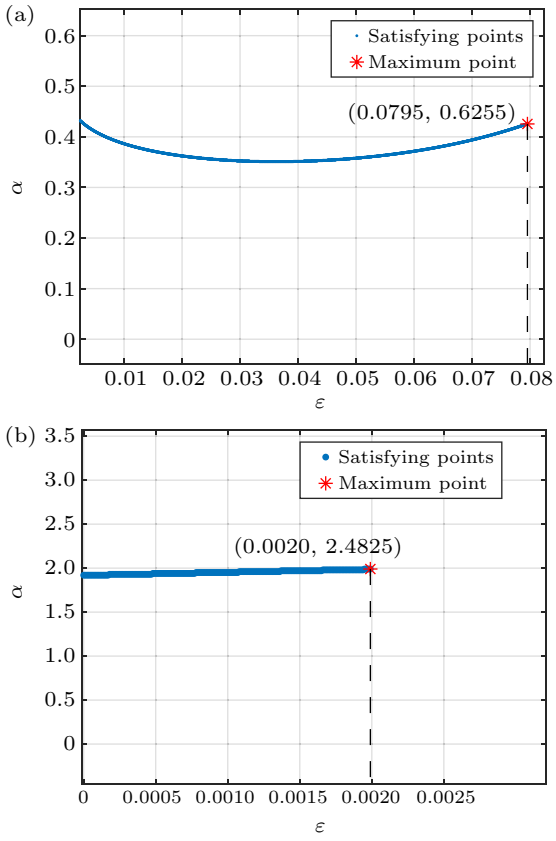


Fig. 5. The x-axis represents the error parameter ε in the lab measurement, and the y-axis represents the minimum parameter α corresponding to the case where the Bell-type witness operators $\mathcal{B}$ can still distinguish the network topology in the lab measurement. (a) When $\alpha\le f_1(\varepsilon)$, the maximum point of 0.0795 indicates that the witness operator can tolerate a maximum measurement error of 0.0795 at this time. (b) When $\alpha>f_1(\varepsilon)$, the maximum allowable measurement error is only 0.0020.

Figure 5 illustrates the minimum value of the parameter α that can be chosen for different levels of inaccuracy ε. When $\alpha\le f_1(\varepsilon)$, based on numerical calculations, we find that the error range should be controlled within $[0,0.0795]$. Based on the results in Fig. 5(a), we can further adjust the value of α accordingly. In this case, the Bell-type witness operator $\mathcal{B}$ remains effective for distinguishing network topologies. Similarly, when $\alpha>f_1(\varepsilon)$, we obtain analogous results.

Secondly, we investigate how the detection efficiency η affects the discrimination of the network topology using Bell-type witness operator $\mathcal{B}$. Considering network topologies shown in Figs. 1(b)–1(e), the distribution of sources in each network and the chosen ideal measurements are the same as those discussed earlier. We further demonstrate that the detection efficiency η will also affect the upper bound of $\langle\mathcal{B}\rangle$. For example, for the quantum network N_1 depicted in Fig. 1(b), we assume that parties Alice and Bob share a state $|\Phi^+\rangle_{AB}=(|00\rangle_{AB}+|11\rangle_{AB})/\sqrt{2}$. Under the influence of the detection efficiency η, we can obtain

$$\begin{aligned}&\alpha(\langle A_0B_0(C_0+C_1)\rangle+\langle A_1B_1(C_0-C_1)\rangle)\\&\quad+\langle A_0(C_0+C_1)\rangle+\langle A_0(C_0-C_1)\rangle=2(\alpha+1),\end{aligned}\tag{41}$$

$$\begin{aligned}&\alpha(\langle A_2(B_2+B_3)C_2\rangle+\langle A_2(B_2-B_3)C_2\rangle)\\&\quad+\langle(B_2+B_3)C_2\rangle+\langle(B_2-B_3)C_2\rangle=2(\alpha+1)\end{aligned}\tag{42}$$

from Eqs. (32), (35), and (36),

$$\begin{aligned}&\alpha(\langle A_2(B_2+B_3)C_2\rangle+\langle A_2(B_2-B_3)C_2\rangle)+\langle(B_2+B_3)C_2\rangle\\&\quad+\langle(B_2-B_3)C_2\rangle=2\sqrt{2}\eta^2\alpha\end{aligned}\tag{43}$$

from Eqs. (33)–(36),

$$\begin{aligned}&\alpha(\langle(A_4+A_5)B_4C_4\rangle+\langle(A_4-A_5)B_4C_4\rangle)\\&\quad+\langle(A_4+A_5)B_4\rangle+\langle(A_4-A_5)B_4\rangle=2\sqrt{2}\eta^2(\alpha+1).\end{aligned}\tag{44}$$

Thus we get

$$S'_{N_1}=\begin{cases}(\alpha+1)(4+2\sqrt{2}\eta^2), & \text{if } \alpha\le f_2(\eta),\\ 2\sqrt{2}\eta^2(2\alpha+1)+2(\alpha+1), & \text{if } \alpha>f_2(\eta).\end{cases}$$

We then consider the upper bound of $\langle\mathcal{B}\rangle$ in other cases and list these upper bounds in Table 5.

Table 5. In different realizations of triangle network, the table shows the upper bound of S'_{N_m} under the influence of detection efficiency η. Here $f_2(\eta)=1/(\sqrt{2}\eta^2-1)$.

Network topology	Upper bound S'_{N_m}
N_0	$S'_{N_0}=6\alpha+6$
N_1	$S'_{N_1}=\begin{cases}(\alpha+1)(4+2\sqrt{2}\eta^2), & \text{if } \alpha\le f_2(\eta),\\ 2\sqrt{2}\eta^2(2\alpha+1)+2(\alpha+1), & \text{if } \alpha>f_2(\eta)\end{cases}$
$N_{1'}$	$S'_{N_{1'}}=6\sqrt{(\eta^2+\alpha\eta^3)^2+(\alpha\eta^3)^2}$
N_2	$S'_{N_2}=\begin{cases}(4\sqrt{2}\eta^2+2)(\alpha+1), & \text{if } \alpha\le f_2(\eta),\\ 6\sqrt{2}\eta^2\alpha+4\sqrt{2}\eta^2, & \text{if } \alpha>f_2(\eta)\end{cases}$
N_3	$S'_{N_3}=6\sqrt{2}\eta^2(\eta\alpha+1)$

To analyze how measurement detection efficiency η impacts the discrimination of network topologies, we must adjust the parameter α of the Bell-type witness operator $\mathcal{B}$ for different values of η. Specifically, if $\alpha\le f_2(\eta)$, using numerical

calculations, we find that for certain detection efficiencies η, simply adjusting the parameter α allows the Bell-type witness operator $\mathcal{B}$ to still distinguish network topologies. For example, Fig. 6(a) shows that the network topology shown in Fig. 1 can be distinguished using $\mathcal{B}$ when $\eta \geq 0.947$. If $\alpha > f_2(\eta)$, Fig. 6(b) illustrates the minimum values of α required for different detection efficiencies. Notably, when $\eta < 0.944$, the method of using $\mathcal{B}$ to distinguish between network topologies fails regardless of the value of α.

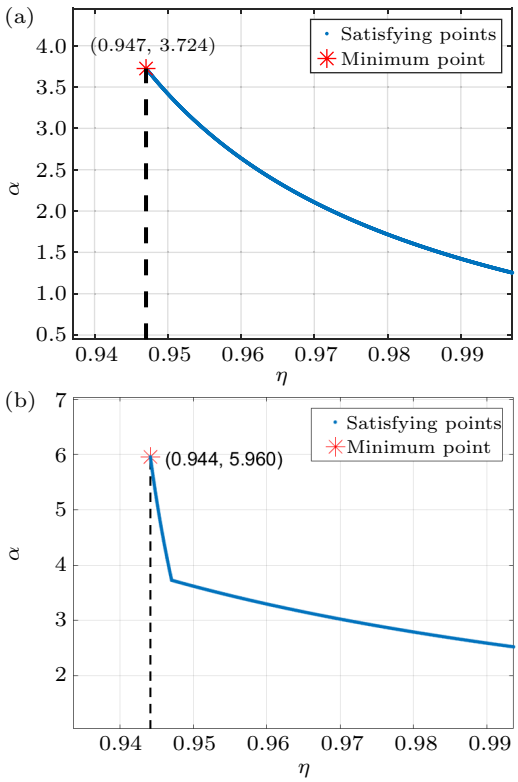


Fig. 6. The x-axis represents the detector efficiency of the measurement, η, and the y-axis represents the minimum parameter α corresponding to the case where the Bell-type witness operators $\mathcal{B}$ can still distinguish the network topology in the lab measurement. (a) In the case of $\alpha \leq f_2(\eta)$, the minimum success efficiency of the detector is 0.947. (b) In the case of $\alpha > f_2(\eta)$, the minimum success efficiency of the detector is 0.944.

5. Discussion and conclusion

In this paper, for a star network comprising four parties, we present Bell-type inequalities that can determine the number of quantum sources in the network topology. By integrating the results of the CHSH inequality, we can precisely determine the location of each source. In fact, the method we propose can be generalized to star networks with n parties. More importantly, we investigate how two distinct types of measurement imprecision impact topology distinguishability within star and triangle quantum networks. Our study establishes robust error thresholds for reliable network topology discrimination.

In addition, one can analyze the problem of distinguishing network topologies under different structures using a similar method that combines and tests the violation of various Bell-type inequalities. For specific network structures, exploring different forms of Bell-type inequalities in future work may lead to a more robust method for distinguishing network topologies.

Appendix A

Consider the network M_1 shown in Fig. 2(b), and assume that parties A and D share a quantum state $|\Phi^+\rangle_{AD} = (|00\rangle_{AD} + |11\rangle_{AD})/\sqrt{2}$. If the observables performed by parties A and D correspond to Eqs. (19)–(20), the measurement schemes performed by parties B and C always ensure that Eqs. (21) and (22) hold, we obtain

$$|\langle A^+ D_0 B_1^+\rangle|^{1/2} + |\langle A^- D_1 B_1^-\rangle|^{1/2} = 2^{5/4}, \tag{A1}$$

$$|\langle A^+ D_2 C_1^+\rangle|^{1/2} + |\langle A^- D_3 C_1^-\rangle|^{1/2} = 2^{5/4}, \tag{A2}$$

$$|\langle B_2^+ D_4 C_2^+\rangle|^{1/2} + |\langle B_2^- D_5 C_2^-\rangle|^{1/2} = 2. \tag{A3}$$

Combining with Eqs. (A1)–(A3) we obtain that $S_{M_1} = 2 + 2^{9/4}$.

For other network topologies, the value of S_{M_n} can also be obtained using similar calculation methods. For the quantum network depicted in Fig. 2(c), we assume that parties A and D share a state $|\Phi^+\rangle_{AD} = (|00\rangle_{AD} + |11\rangle_{AD})/\sqrt{2}$, and parties B and D share a state $|\Phi^+\rangle_{BD'} = (|00\rangle_{BD'} + |11\rangle_{BD'})/\sqrt{2}$. The selected measurement scheme is defined as follows:

$$A_0 = \frac{1}{\sqrt{2}}(\sigma_z + \sigma_x),\ A_1 = \frac{1}{\sqrt{2}}(\sigma_z - \sigma_x), \tag{A4}$$

$$B_{10} = B_{20} = \frac{1}{\sqrt{2}}(\sigma_z + \sigma_x), \tag{A5}$$

$$B_{11} = B_{21} = \frac{1}{\sqrt{2}}(\sigma_z - \sigma_x), \tag{A6}$$

$$D_0 = \sigma_z \otimes \sigma_z,\ D_1 = \sigma_x \otimes \sigma_x, \tag{A7}$$

$$D_2 = D_4 = \sigma_z \otimes I_2,\ D_3 = D_5 = \sigma_x \otimes I_2. \tag{A8}$$

Meanwhile, for party C, who receives only classical variables, measurements can always be selected to ensure that $\langle C_{10}\rangle = \langle C_{20}\rangle = 1$ and $\langle C_{11}\rangle = \langle C_{21}\rangle = 0$ hold. Thus, we derive an upper bound of $\langle \mathcal{Q}\rangle$ as $S_{M_2} = 2\sqrt{2} + 2^{9/4}$.

For the quantum network shown in Fig. 2(d), we suppose that parties A and D, parties B and D, and parties C and D share the entangled states $|\Phi^+\rangle_{AD} = (|00\rangle_{AD} + |11\rangle_{AD})/\sqrt{2}$, $|\Phi^+\rangle_{BD'} = (|00\rangle_{BD'} + |11\rangle_{BD'})/\sqrt{2}$, and $|\Phi^+\rangle_{CD''} = (|00\rangle_{CD''} + |11\rangle_{CD''})/\sqrt{2}$, respectively. The corresponding measurement scheme is defined as follows:

$$A_0 = B_{10} = B_{20} = C_{10} = C_{20} = \frac{1}{\sqrt{2}}(\sigma_z + \sigma_x), \tag{A9}$$

$$A_1 = B_{11} = B_{21} = C_{11} = C_{21} = \frac{1}{\sqrt{2}}(\sigma_z - \sigma_x), \tag{A10}$$

$$D_0 = \sigma_z \otimes \sigma_z \otimes I_2,\ D_1 = \sigma_x \otimes \sigma_x \otimes I_2, \tag{A11}$$

$$D_2 = \sigma_z \otimes I_2 \otimes \sigma_z,\ D_3 = \sigma_x \otimes I_2 \otimes \sigma_x, \tag{A12}$$

$$D_4 = I_2 \otimes \sigma_z \otimes \sigma_z,\ D_5 = I_2 \otimes \sigma_x \otimes \sigma_x, \tag{A13}$$

We determine the upper bound of $\langle \mathcal{Q} \rangle$ as $6\sqrt{2}$.

Appendix B

Consider the quantum network depicted in Fig. 2(b), where parties A and D share a quantum state $|\Phi^+\rangle_{AD} = (|00\rangle_{AD} + |11\rangle_{AD})/\sqrt{2}$. By analyzing the measurement scheme described in Eqs. (19) and (20), we can find that the local measurements of parties A and D always involve σ_x, σ_z, $\frac{1}{\sqrt{2}}(\sigma_z + \sigma_x)$ and $\frac{1}{\sqrt{2}}(\sigma_z - \sigma_x)$. Given that the imprecision of each measurement is ε, we can use Eqs. (23)–(26) to express the measurement scheme as follows:

$$\tilde{A}_0 = \cos\theta_3 \sigma_z + \sin\theta_3 \sigma_x, \tag{B1}$$

$$\tilde{A}_1 = \cos\theta_3 \sigma_z - \sin\theta_3 \sigma_x, \tag{B2}$$

$$\tilde{D}_0 = \tilde{D}_2 = \cos\theta_1 \sigma_z + \sin\theta_1 \sigma_x, \tag{B3}$$

$$\tilde{D}_1 = \tilde{D}_3 = \cos\theta_2 \sigma_z + \sin\theta_2 \sigma_x, \tag{B4}$$

where $\theta_1 = \arcsin(1-2\varepsilon)$, $\theta_2 = \arccos(1-2\varepsilon)$, and $\theta_3 = \arcsin(1-2\varepsilon) - \pi/4$. Since parties B and D only receive classical variables, we can select a measurement scheme such that

$$\langle B_{10} \rangle = \langle B_{20} \rangle = \langle B_{21} \rangle = 1,\ \langle B_{11} \rangle = 0, \tag{B5}$$

$$\langle C_{10} \rangle = \langle C_{20} \rangle = \langle C_{21} \rangle = 1,\ \langle C_{11} \rangle = 0, \tag{B6}$$

are satisfied. Meanwhile, select the measurement where

$$D_4 = D_5 = I_2. \tag{B7}$$

Based on the above discussion, we can calculate that

$$\begin{aligned}
&|\langle A^+ D_0 B_1^+ \rangle|^{1/2} + |\langle A^- D_1 B_1^- \rangle|^{1/2} \\
=\ &|\langle A^+ D_0 \rangle|^{1/2} + |\langle A^- D_1 \rangle|^{1/2} \\
=\ &|2\cos\theta_3 \sigma_z \otimes (\cos\theta_1 \sigma_x + \sin\theta_1 \sigma_z)|^{1/2} \\
&+|2\sin\theta_3 \sigma_x \otimes (\cos\theta_2 \sigma_x + \sin\theta_2 \sigma_z)|^{1/2} \\
=\ &\sqrt{2}\left(|\cos\theta_3 \sin\theta_1|^{1/2} + |\sin\theta_3 \cos\theta_2|^{1/2}\right) \\
=\ &\sqrt{2}(1-2\varepsilon)^{1/2}\left(|\cos\theta_3|^{1/2} + |\sin\theta_3|^{1/2}\right) \\
=\ &2^{3/4}\sqrt{(1-2\varepsilon)^2 + (1-2\varepsilon)(1-8\varepsilon+8\varepsilon^2)^{1/2}},
\end{aligned} \tag{B8}$$

where the last equality holds when $\cos\theta_3 = [k + (2-k^2)^{1/2}]/2$ and $\sin\theta_3 = [k - (2-k^2)^{1/2}]/2$ (or $\cos\theta_3 = [k - (2-k^2)^{1/2}]/2$ and $\sin\theta_3 = [k + (2-k^2)^{1/2}]/2$) with $k = \sqrt{2}(1-2\varepsilon)$ and $1 - 2\varepsilon > 1/\sqrt{2}$. Similarly, we get

$$\begin{aligned}
&|\langle A^+ D_2 C_1^+ \rangle|^{1/2} + |\langle A^- D_3 C_1^- \rangle|^{1/2} \\
=\ &2^{3/4}\sqrt{(1-2\varepsilon)^2 + (1-2\varepsilon)(1-8\varepsilon+8\varepsilon^2)^{1/2}}.
\end{aligned}$$

In fact, since the variables shared between parties B and D, as well as between parties D and C, are classical, we have

$$|\langle B_2^+ D_4 C_2^+ \rangle|^{1/2} + |\langle B_2^- D_5 C_2^- \rangle|^{1/2} = 2. \tag{B9}$$

Based on the preceding discussion, we can obtain $S_{M_1} = 2 + 2^{7/4}\sqrt{(1-2\varepsilon)^2 + (1-2\varepsilon)(1-8\varepsilon+8\varepsilon^2)^{1/2}}$.

Using the same methods as above, the corresponding values of S_{M_n} can also be derived for other scenarios.

Appendix C

From the structure of $\mathcal{B}$, it is evident that all terms in $\mathcal{B}$ are either Mermin-type or CHSH-type operators. The optimal quantum bound for these operators arises from local measurements performed on the EPR state.[39] Hence, due to linearity, it is sufficient to determine the bound of $\langle \mathcal{B} \rangle$ using the EPR state. Suppose that Alice and Bob share an EPR state $|\Phi^+\rangle_{AB} = (|00\rangle_{AB} + |11\rangle_{AB})/\sqrt{2}$. Ideally, each party should perform the measurement scheme shown in Eqs. (31)–(36). However, in practice, we consider the imprecise measurements shown in Eqs. (37)–(40), and we can calculate the corresponding values

$$\begin{aligned}
&\alpha(\langle A_0 B_0 (C_0 + C_1) \rangle + \langle A_1 B_1 (C_0 - C_1) \rangle) + \langle A_0 (C_0 + C_1) \rangle \\
&+\langle A_0 (C_0 - C_1) \rangle = 2(\alpha + 1),
\end{aligned} \tag{C1}$$

$$\alpha(\langle A_2 (B_2 + B_3) C_2 \rangle + \langle A_2 (B_2 - B_3) C_2 \rangle) \tag{C2}$$

$$+\langle (B_2 + B_3) C_2 \rangle + \langle (B_2 - B_3) C_2 \rangle = 2(\alpha + 1) \tag{C3}$$

from Eqs. (32), (35), and (36),

$$\begin{aligned}
&\alpha(\langle A_2 (B_2 + B_3) C_2 \rangle + \langle A_2 (B_2 - B_3) C_2 \rangle) \\
&+\langle (B_2 + B_3) C_2 \rangle + \langle (B_2 - B_3) C_2 \rangle \\
&= 2\sqrt{2}\alpha(1-2\varepsilon)^2
\end{aligned} \tag{C4}$$

from Eqs. (33)–(36),

$$\begin{aligned}
&\alpha(\langle (A_4 + A_5) B_4 C_4 \rangle + \langle (A_4 - A_5) B_4 C_4 \rangle) + \langle (A_4 + A_5) B_4 \rangle \\
&+\langle (A_4 - A_5) B_4 \rangle = (1+\alpha) 2\sqrt{2}(1-2\varepsilon)^2.
\end{aligned} \tag{C5}$$

Combining Eqs. (C1)–(C5), we obtain

$$S_{N_1} = \begin{cases} (\alpha+1)[2\sqrt{2}(1-2\varepsilon)^2 + 4], & \text{if } \alpha \le f_1(\varepsilon), \\ (2\alpha+1)[2\sqrt{2}(1-2\varepsilon)^2 + 1] + 1, & \text{if } \alpha > f_1(\varepsilon), \end{cases}$$

where $f_1(\varepsilon) = 1/[\sqrt{2}(1-2\varepsilon)^2 - 1]$.

Next, when the local measurements performed by the parties involve σ_z, σ_x, $w_1 = (\sigma_z + \sigma_x)/\sqrt{2}$ and $w_2 = (\sigma_z - \sigma_x)/\sqrt{2}$, they can always be expressed as

$$\tilde{\sigma}_z = \cos\theta_1 \sigma_x + \sin\theta_1 \sigma_z, \tag{C6}$$

$$\tilde{\sigma}_x = \cos\theta_2 \sigma_x + \sin\theta_2 \sigma_z, \tag{C7}$$

$$\tilde{w}_1 = \cos\theta_3 \sigma_x + \sin\theta_3 \sigma_z, \tag{C8}$$

$$\tilde{w}_2 = \cos\theta_4 \sigma_x - \sin\theta_4 \sigma_z, \tag{C9}$$

where $\theta_1 = \arcsin(1-2\varepsilon)$, $\theta_2 = \arccos(1-2\varepsilon)$, $\cos\theta_3 + \sin\theta_3 = \sqrt{2}(1-2\varepsilon)$, and $\theta_3 = \theta_4$.

Case 2 For the network topology $N_{1'}$, Alice, Bob, and Charlie share a tripartite maximally entangled GHZ state $|GHZ\rangle = (|000\rangle + |111\rangle)/\sqrt{2}$. Especially, define quantum observables for each party as

$$A_0 = \sigma_z,\ A_1 = \sigma_x,\ A_2 = I_2,\ A_3 = \sigma_x,$$
$$A_4 = \cos\theta\sigma_z + \sin\theta\sigma_x,\ A_5 = \cos\theta\sigma_z - \sin\theta\sigma_x,$$
$$B_0 = I_2,\ B_1 = \sigma_x,\ B_2 = \cos\theta\sigma_z + \sin\theta\sigma_x,$$
$$B_3 = \cos\theta\sigma_z - \sin\theta\sigma_x,\ B_4 = \sigma_z,\ B_5 = \sigma_x,$$
$$C_0 = \cos\theta\sigma_z + \sin\theta\sigma_x,\ C_1 = \cos\theta\sigma_z - \sin\theta\sigma_x,$$
$$C_2 = \sigma_z,\ C_3 = \sigma_x,\ C_4 = I_2,\ C_5 = \sigma_x.$$

Here $\theta = \arcsin((\alpha+1)/(2\alpha^2+2\alpha+1)^{1/2})$. Therefore, under the influence of measurement errors ε, we can obtain

$$S_{N_{1'}} = 6[(\alpha+1)(1-2\varepsilon)\cos\theta_5 + 2\alpha(1-2\varepsilon)^2\sin\theta_5],$$

where $\theta_5 = \theta - \arccos(1-2\varepsilon)$, $\theta = \arcsin((\alpha+1)/(2\alpha^2+2\alpha+1)^{1/2})$. It is worth noting that the imprecise measurements of $A_4 = C_0$ and $A_5 = C_1$ are assumed to be

$$\tilde{A}_4 = \tilde{C}_0 = \cos\theta_6\sigma_z + \sin\theta_6\sigma_x, \tag{C10}$$
$$\tilde{A}_5 = \tilde{C}_1 = \cos\theta_7\sigma_z - \sin\theta_7\sigma_x, \tag{C11}$$

respectively. Due to the constraints of the imprecision ε, we require $\theta_6 = \theta_7 = \theta - \arccos(1-2\varepsilon)$ with $\theta = \arcsin((\alpha+1)/(2\alpha^2+2\alpha+1)^{1/2})$.

Case 3 For the network topology N_2, suppose that Alice and Bob, and Alice and Charlie share one EPR state $|\Phi^+\rangle_{AB} = (|00\rangle_{AB} + |11\rangle_{AB})/\sqrt{2}$ and $|\Phi^+\rangle_{A'C} = (|00\rangle_{A'C} + |11\rangle_{A'C})/\sqrt{2}$ respectively. In the ideal case, considering the observables shown in Eqs. (S31)–(S33) from the supplementary material of Ref. [30]. After performing imprecise measurements during the experiment, we find that

$$S_{N_2} = \begin{cases} 2\alpha+2+4\sqrt{2}(1-2\varepsilon)^2(\alpha+1), & \text{if } \alpha \le f_1(\varepsilon), \\ 2\sqrt{2}(1-2\varepsilon)^2(3\alpha+2), & \text{if } \alpha > f_1(\varepsilon), \end{cases}$$

where $f_1(\varepsilon) = 1/[\sqrt{2}(1-2\varepsilon)^2 - 1]$.

Case 4 For the network topology N_3, suppose that Alice, Bob and Charlie share three EPR states $|\Phi^+\rangle_{AB} = (|00\rangle_{AB} + |11\rangle_{AB})/\sqrt{2}$, $|\Phi^+\rangle_{A'C} = (|00\rangle_{A'C} + |11\rangle_{A'C})/\sqrt{2}$, and $|\Phi^+\rangle_{B'C'} = (|00\rangle_{B'C'} + |11\rangle_{B'C'})/\sqrt{2}$, respectively. If under ideal conditions each party performs the measurement as Eq. (S47) in the supplementary material of Ref. [30], then, considering the influence of noise on the measurements performed in the experiment, we can still obtain

$$S_{N_3} = 6\sqrt{2}(1-2\varepsilon)^2(\alpha+1). \tag{C12}$$

Acknowledgments

Project supported by the National Natural Science Foundation of China (Grant Nos. 12271394 and 62172341) and the Sichuan Natural Science Foundation (Grant Nos. 2024NSFSC1365 and 2024NSFSC1375).

References

[1] Lago-Rivera D, Rakonjac J V, Grandi S and de Riedmatten H 2023 *Nat. Commun.* **14** 1889
[2] Cirac J I, Ekert A K, Huelga S F and Macchiavello C 1999 *Phys. Rev. A* **59** 4249
[3] Gisin N and Thew R 2007 *Nat. Photonics* **1** 165
[4] Kimble H J 2008 *Nature* **453** 1023
[5] Scarani V, H B P, Cerf N J, Dušek M, Lütkenhaus N and Peev M 2009 *Rev. Mod. Phys.* **81** 1301
[6] Proctor T J, Knott P A and Dunningham J A 2018 *Phys. Rev. Lett.* **120** 080501
[7] Xu F, Ma X, Zhang Q, Lo H K and Pan J W 2020 *Rev. Mod. Phys.* **92** 025002
[8] Chen Y A, Zhang Q Z, Chen T Y, Cai W Q, Liao S K, Zhang J, Chen K, Yin J, Ren J G, Chen Z, Han S L, Yu Q, Liang K, Zhou F, Yuan X, Zhao M S, Wang T Y, Jiang X, Zhang L, Liu W Y, Li Y, Shen Q, Cao Y, Lu C Y, Shu R, Wang J Y, Li L, Liu N L, Xu F, Wang X B, Peng C Z and Pan J W 2021 *Nature* **589** 214
[9] Zhang Z and Zhang Q 2021 *Quantum Sci. Technol.* **6** 043001
[10] Clauser J F, Horne M A, Shimony A and Holt R A 1969 *Phys. Rev. Lett.* **23** 880
[11] Fang K, Zhao J T, Li X F, Li Y F and Duan R Y 2023 *Sci. China Inf. Sci* **66** 180509
[12] Collins O A, Jenkins S D, Kuzmich A and Kennedy T A B 2007 *Phys. Rev. Lett.* **98** 060502
[13] Weinbrenner L T, Vandré L, Coopmans T and Gühne O 2024 *Phys. Rev. A* **109** 052611
[14] Shchukin E, Schmidt F and Loock P V 2019 *Phys. Rev. A* **100** 032322
[15] Hu X M, Zhang C, Guo Y, Wang F X, Xing W B, Huang C X, Liu B H, Huang Y F, Li C F, Guo G C, Gao X, Pivoluska M and Huber M 2021 *Phys. Rev. Lett.* **127** 110505
[16] Ma H Y, Qin G Q, Fan X K and Chu P C 2015 *Acta Phys. Sin.* **64** 160306 (in Chinese)
[17] Yang X, Yang Y H and Luo M X 2022 *Phys. Rev. Res.* **4** 013153
[18] Chen D T, Doolittle B, Larson J, Saleem Z H and Chitambar E 2023 *PRX Quantum* **4** 040347
[19] Weinbrenner L T, Prasannan N, Hansenne K, Denker S, Sperling J, Brecht B, Silberhorn C and Gühne O 2024 *Phys. Rev. Lett.* **132** 240802
[20] Chaves R 2016 *Phys. Rev. Lett.* **116** 010402
[21] Rosset D, Branciard C, Barnea T J, Pütz G, Brunner N and Gisin N 2016 *Phys. Rev. Lett.* **116** 010403
[22] Gisin N, Mei Q, Tavakoli A, Renou M O and Brunner N 2017 *Phys. Rev. A* **96** 020304
[23] Luo M X 2018 *Phys. Rev. Lett.* **120** 140402
[24] Tavakoli A, Gisin N and Branciard C 2021 *Phys. Rev. Lett.* **126** 220401
[25] Supić I, Bancal J D, Cai Y and Brunner N 2022 *Phys. Rev. A* **105** 022206
[26] Pozas-Kerstjens A, Gisin N and Tavakoli A 2022 *Phys. Rev. Lett.* **128** 010403
[27] Wang N N, Yang X, Yang Y H, Zhang C, Luo M X, Liu B H, Huang Y F, Li C F and Guo G C 2025 *Phys. Rev. Lett.* **134** 080202
[28] Luo M X, Yang X and Pozas-Kerstjens A 2024 *Phys. Rev. A* **110** 022617
[29] Luo M X and Fei S M 2024 *Adv. Quantum Tech.* **7** 2400021
[30] Mao Y L, Chen H, Guo B X, Liu S T, Li Z D, Luo M X and Fan J Y 2024 *Phys. Rev. Lett.* **132** 240801
[31] Yang S Y, He K, Hou J C, Ma Z H, Fei S M and Luo M X 2024 *Phys. Rev. A* **110** 032437
[32] Rosset D, Ferretti-Schöbitz R, Bancal J D, Gisin N and Liang Y C 2012 *Phys. Rev. A* **86** 062325
[33] James D F V, Kwiat P G, Munro W J and White A G 2001 *Phys. Rev. A* **64** 052312
[34] Moroder T, Gühne O, Beaudry N, Piani M and Lütkenhaus N 2010 *Phys. Rev. A* **81** 052342
[35] Morelli S, Yamasaki H, Huber M and Tavakoli A 2022 *Phys. Rev. Lett.* **128** 250501
[36] Tavakoli A 2024 *Phys. Rev. Lett.* **132** 070204
[37] Cao H, Morelli S, Rozema L A, Zhang C, Tavakoli A and Walther P 2024 *Phys. Rev. Lett.* **133** 150201
[38] Clauser J F, Horne M A, Shimony A and Holt R A 1969 *Phys. Rev. Lett.* **23** 880
[39] Einstein A, Podolsky B and Rosen N 1935 *Phys. Rev.* **47** 777